CHEMISTRY
A EUROPEAN JOURNAL

DOI: 10.1002/chem.200701440

Explorations of New Types of Second-Order Nonlinear Optical Materials in Cd(Zn)-V^{V}-Te^{IV}-O Systems

Hai-Long Jiang,[a, b] Shu-Ping Huang,[a, b] Yang Fan,[a, b] Jiang-Gao Mao,*[a] and Wen-Dan Cheng[a]

Abstract: Solid-state reactions of zinc(II) or cadmium(II) oxide, V_2O_5, and TeO_2 at high temperature led to two novel quaternary compounds, namely, $Zn_3V_2TeO_{10}$ and $Cd_4V_2Te_3O_{15}$. The structure of $Zn_3V_2TeO_{10}$ is a complicated three-dimensional (3D) network constructed by the interconnection of ZnO_5, ZnO_6, VO_4, and TeO_4 polyhedra via corner- and edge-sharing. $Cd_4V_2Te_3O_{15}$ with an acentric structure features a 3D network in which the cadmium tellurite layers are further interconnected by both "isolated" VO_4 tetrahedra and one-dimensional (1D) vanadium oxide helical chains. $Cd_4V_2Te_3O_{15}$ displays a second harmonic generation (SHG) efficiency of about 1.4 times that of KH_2PO_4 (KDP). Both compounds are direct band-gap semiconductors and are transparent in the range of 0.6–10.0 μm. Measurements of luminescence indicate that both compounds exhibit broad emission bands in the blue-light region.

Keywords: density functional calculations · noncentrosymmetric (ncs) · nonlinear optics · solid-state reactions

Introduction

The search for new second-order nonlinear optical (NLO) materials is of current interest and great importance due to their applications in photonic technologies.[1] Currently, the most widely used such materials are inorganic crystals based on borates, such as β-BaB_2O_4 (BBO) and LiB_3O_5 (LBO), and phosphates, such as KH_2PO_4 (KDP) and $KTiOPO_4$ (KTP).[2] It is reported that the π-conjugated system based on trigonal BO_3 groups is responsible for the second harmonic generation (SHG) properties of the borates.[1,3] Studies have shown that the asymmetric coordination polyhedron adopted by Se^{IV} or Te^{IV} atoms with a lone pair can also induce noncentrosymmetric structures (NCS) which might be SHG effective.[4–7] Transition-metal ions with a d^0 electronic configuration, such as Ti^{4+}, V^{5+}, Nb^{5+}, W^{6+}, Mo^{6+}, which are susceptible to second-order Jahn–Teller distortions have been introduced to the metal selenite or tellurite systems to improve their SHG properties.[4–7] Recently we found that the combination of B–O and Se–O bonds can also afford a new type of second-order NLO compound.[7c] Most such studies apply NH_4^+, alkali- or alkaline-earth-metal ions as cations, therefore such materials are usually insulators which may be used in the ultraviolet or the vacuum ultraviolet region.[1–8] On the other hand, semiconducting second-order NLO materials such as CdSe and $AgGaSe_2$ are also urgently required because they can be used in the mid-wave (2–5 μm) and farwave (>5 μm) infrared region.[9] These materials have been used in applications in optical parametric oscillation (OPO) and in blue- and green-light laser devices.[9] However, currently such materials are relatively few and mostly limited to transition-metal chalcogenides the large-sized single crystals of which are difficult to grow. We deem that the replacement of the alkaline-earth or alkali-metal ions (A) in the A–d^0 transition-metal ion–Te^{IV} (or Se^{IV})–O systems by d^{10} ions, such as zinc(II) or cadmium(II), may greatly reduce the band gaps to form new types of semiconducting SHG materials that are transparent in the IR region. Our research efforts in the almost unexplored Zn(Cd)-V^{V}-Te^{IV}-O systems afforded two new quaternary phases, namely, $Zn_3V_2TeO_{10}$ and $Cd_4V_2Te_3O_{15}$.

[a] H.-L. Jiang, S.-P. Huang, Y. Fan, Prof. J.-G. Mao, Prof. W.-D. Cheng
State Key Laboratory of Structural Chemistry
Fujian Institute of Research on the Structure of Matter
Chinese Academy of Sciences, Fuzhou 350002 (China)
Fax: (+86) 591-8371-4946
E-mail: mjg@fjirsm.ac.cn

[b] H.-L. Jiang, S.-P. Huang, Y. Fan
Graduate School of the Chinese Academy of Sciences
Beijing 100039 (China)

Supporting information for this article is available on the WWW under http://www.chemeurj.org/ or from the author.

$Cd_4V_2Te_3O_{15}$ is a second-order NLO material with a moderately strong SHG efficiency of about 1.4 times that of KH_2PO_4 (KDP) and it is transparent in the IR region. Herein we report their syntheses, crystal, and band structures, as well as optical properties.

Results and Discussion

Exploration of the new types of NLO materials in the Zn(Cd)-V^V-Te^{IV}-O systems led to the isolation of two novel zinc(II) or cadmium(II) vanadium(V) tellurium(IV) oxides, namely, $Zn_3V_2TeO_{10}$ and $Cd_4V_2Te_3O_{15}$. Both compounds feature a complicated 3D network structure and $Cd_4V_2Te_3O_{15}$ shows a moderately strong second-order SHG response and it is transparent in the IR region.

Structural descriptions: The synthesis of $Zn_3V_2TeO_{10}$ can be expressed by reaction (1) at 670 °C:

$$3\,ZnO + V_2O_5 + TeO_2 \rightarrow Zn_3V_2TeO_{10} \quad (1)$$

$Zn_3V_2TeO_{10}$ features a three-dimensional (3D) network structure composed of ZnO_5, ZnO_6, VO_4, and TeO_4 polyhedra interconnected via corner- and edge-sharing (Figure 1). The asymmetric unit of $Zn_3V_2TeO_{10}$ contains

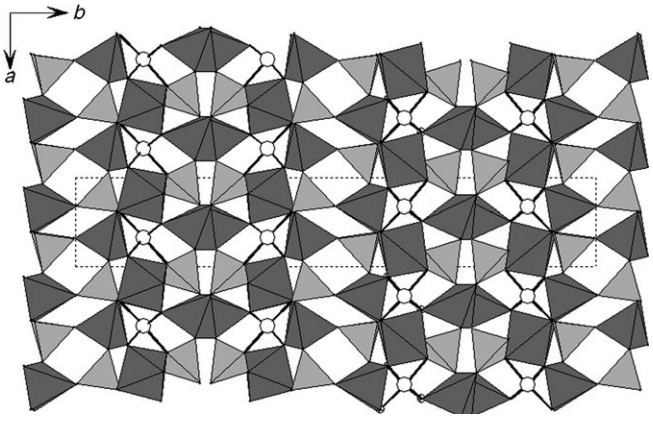

Figure 1. View of the structure of $Zn_3V_2TeO_{10}$ looking down the *c* axis. The ZnO_5 and ZnO_6 polyhedra are shaded in medium gray and VO_4 tetrahedra are shaded in light gray. Te and O atoms are drawn as open and crossed circles, respectively.

three unique zinc(II) atoms, two unique vanadium(V) atoms, and a tellurium(IV) atom. The Zn1 atom is octahedrally coordinated by six oxygen atoms, whereas the Zn2 and Zn3 atoms are five-coordinate in a distorted trigonal-bipyramidal geometry (Figure 2). The Zn–O distances are in the range of 1.905(5)–2.462(4) Å (Table 2), which is comparable to those in the zinc tellurites or tellurates reported.[10,11] Both the vanadium atoms are in a slightly distorted tetrahedral coordination environment surrounded by one oxygen atom from the tellurite group and three terminal oxygen atoms. The V–O distances range from 1.641(5) to

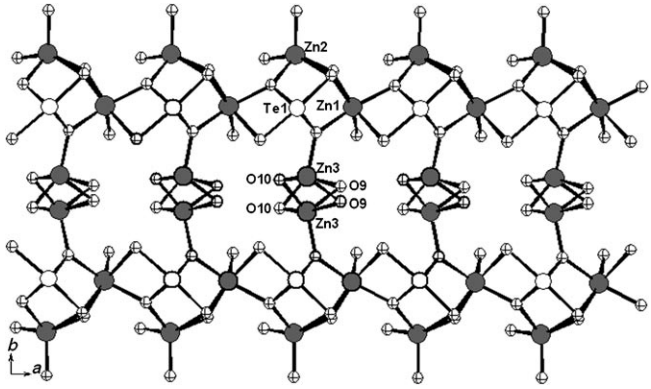

Figure 2. A 2D zinc(II) tellurium(IV) oxide layer in $Zn_3V_2TeO_{10}$.

Table 1. Crystal data and structure refinements for $Zn_3V_2TeO_{10}$ and $Cd_4V_2Te_3O_{15}$.

formula	$Zn_3V_2TeO_{10}$	$Cd_4V_2Te_3O_{15}$
F_w	585.59	1174.28
space group	$P2_1/c$	$P2_12_12_1$
a [Å]	5.2629(5)	5.3993(4)
b [Å]	30.534(3)	16.048(1)
c [Å]	5.5054(5)	16.235(1)
α [°]	90	90
β [°]	98.653(5)	90
γ [°]	90	90
V [Å^3]	874.6(2)	1406.7(2)
Z	4	4
ρ_{calcd} [g cm^{-3}]	4.447	5.545
μ [mm^{-1}]	13.475	13.389
crystal size [mm]	0.15×0.10×0.03	0.30×0.04×0.02
F(000)	1072	2056
Flack parameter		0.01(5)
reflns collected	6620	10877
independent reflns	1998 [R_{int} = 0.0474]	3208 [R_{int} = 0.0365]
obsd data [$I > 2\sigma(I)$]	1715	2903
data/restraints/parameters	1998/0/145	3208/0/218
GOF on F^2	1.065	1.150
$R1$, $wR2$ ($I > 2\sigma(I)$)[a]	0.0361, 0.0848	0.0392, 0.0603
$R1$, $wR2$ (all data)	0.0447, 0.0893	0.0455, 0.0626

[a] $R1 = \Sigma||F_o| - |F_c||/\Sigma|F_o|$, $wR2 = \{\Sigma w[(F_o)^2 - (F_c)^2]^2/\Sigma w[(F_o)^2]^2\}^{1/2}$.

1.817(4) Å (Table 2), comparable to those in other corresponding vanadium compounds reported.[11] The Te1 atom resides in a distorted ψ-TeO_4 tetragonal pyramid with the fifth site occupied by the lone-pair electrons of the tellurium(IV). The Te–O distances are in the range of 1.866(4)–2.085(4) Å. Bond valence calculations indicate that V and Te atoms are in an oxidation state of +5 and +4, respectively. The calculated total bond valences for the V(1), V(2), and Te(1) atoms are 5.07, 5.13, and 4.15, respectively.[12]

Neighboring $Zn(1)O_6$ and $Zn(2)O_5$ polyhedra are interconnected via edge- and corner-sharing into a one-dimensional (1D) chain along the *a* axis. The $Zn(3)O_5$ polyhedra are also interconnected via edge-sharing to form a 1D chain along the *c* axis. The two types of chains are further interconnected via corner-sharing into a thick zinc oxide layer parallel to the *ac* plane. The TeO_4 groups are grafted into the layer above through Te-O-Zn bridges (Figure 2). Such neighboring layers are bridged by $V(1)O_4$ tetrahedra via

corner-sharing along the *b* axis into a 3D architecture. The $V(2)O_4$ tetrahedra are located at the tunnels formed by Zn_6Te_2 eight-membered rings (Figure 1).

The structure of $Zn_3V_2TeO_{10}$ can also be described in terms of the Te atoms occupying the tunnels formed by Zn_4V five-membered rings in the 3D network of zinc(II) vanadium(V) oxide (Figure 3). The Zn_2V three-membered

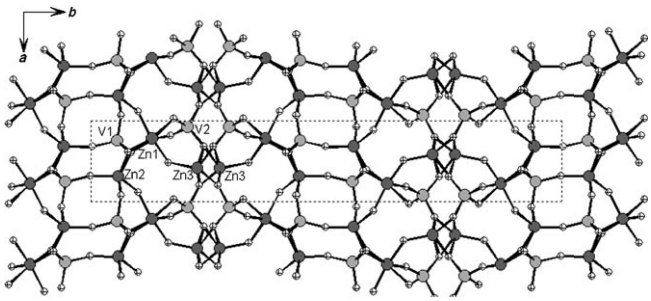

Figure 3. View of the 3D zinc(II) vanadium(V) oxide network looking down the *c* axis in $Zn_3V_2TeO_{10}$.

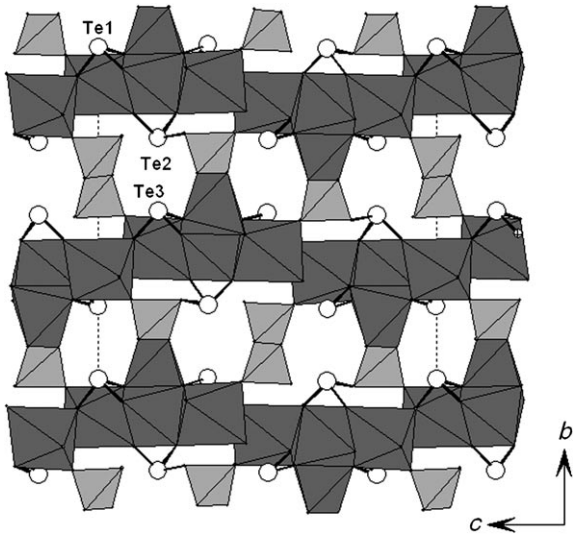

Figure 4. View of the structure of $Cd_4V_2Te_3O_{15}$ looking down the *a* axis. The CdO_6 and VO_4 polyhedra are shaded in medium and light gray, respectively. Te and O atoms are drawn as open and crossed circles, respectively.

rings and Zn_2V_2 four-membered rings are also present in the framework of the zinc(II) vanadium(V) oxide (Figure 3). It is interesting to compare the structure of $Zn_3V_2TeO_{10}$ with the organically covalently bonded zinc(II) vanadium(V) tellurium(IV) oxide, $Zn_2(bipy)_2V_4TeO_{14}$, which we have reported previously.[11b] The structure of $Zn_2(bipy)_2V_4TeO_{14}$ features a layered structure built from 1D double chains of $Zn(bipy)V_3O_9$ interconnected by 1D chains of $Zn(bipy)VTeO_6$ via V-O-Te bridges, the VO_4 tetrahedra are interconnected via corner-sharing into a 1D chain. Obviously, the coordination of bipy to the zinc(II) ion reduces the coordination sites for oxygen atoms, hence the dimensionality of the structure is lowered.[11b]

The synthesis of $Cd_4V_2Te_3O_{15}$ can be expressed by reaction (2) at 610 °C:

$$4\,CdO + V_2O_5 + 3\,TeO_2 \rightarrow Cd_4V_2Te_3O_{15} \qquad (2)$$

The structure of $Cd_4V_2Te_3O_{15}$ features a 3D network in which the cadmium tellurite layers are further interconnected by discrete VO_4 tetrahedra and 1D vanadium oxide helical chains (Figure 4). All four unique cadmium(II) ions are octahedrally coordinated by six oxygen atoms with Cd–O distances ranging from 2.161(7) to 2.615(8) Å. The V(1) atom is tetrahedrally coordinated by four O^{2-} ions, whereas the V(2) atom is tetrahedrally coordinated by one tellurite oxygen and three O^{2-} ions. The V–O distances are in the range of 1.633(7)–1.860(8) Å, which are comparable to those in $Zn_3V_2TeO_{10}$ and previously reported.[11] Neighboring $V(1)O_4$ tetrahedra are further interconnected via corner-sharing into a 1D right-handed helical chain, whereas the $V(2)O_4$ tetrahedra remain "isolated". All three tellurium(IV) atoms in the asymmetric unit are coordinated by three oxygen atoms in a distorted ψ-TeO_3 tetrahedral geometry with the fourth site occupied by the lone-pair electrons which is different to that found for $Zn_3V_2TeO_{10}$. The Te–O distances are in the range of 1.854(8)–1.943(8) Å. For the Te1 atom, there is also an additional greatly elongated Te–O bond (2.525(8) Å) that could be considered as a secondary coordination bond. Bond valence calculations indicate that the V atoms have an oxidation state of +5 and the Te atom has an oxidation state of +4, the calculated total bond valences for V(1), V(2), Te(1), Te(2), and Te(3) are 5.10, 5.05, 4.14, 3.81, and 3.84, respectively.[12]

The CdO_6 octahedra are further interconnected via corner- and edge-sharing into a two-dimensional (2D) cadmium(II) oxide layer based on $\{Cd_5O_{20}\}$ pentamers, in which three oxygen atoms act as μ^3-metal linkers (Figure 5a). These pentamers are further condensed through the sharing of Cd3 atoms along the *a* axis and sharing oxygen corners along the *c* axis into a unique cadmium(II) oxide layer. The tellurite anions cap on both sides of the cadmium(II) oxide layer to form a novel cadmium(II) tellurium(IV) oxide layer (Figure 5b). The above-mentioned cadmium(II) tellurium(IV) oxide layers are bridged by "isolated" $V(2)O_4$ tetrahedra and V(1) oxide helical chains into a 3D architecture with two types of left-handed helical tunnels along the *a* axis (Figure 6). The larger ones are formed by eight-membered rings composed of four cadmium(II) atoms, three vanadium(V) atoms, and a tellurium(IV) atom whereas the smaller ones are formed by six-membered rings containing four cadmium(II) and two vanadium(V) atoms. The lone-pair electrons of the tellurium(IV) atoms are orientated towards the tunnels above. The effective volume of the lone-pair electrons is approximately the same as the volume of an O^{2-} ion according to Galy and Andersson.[13]

Thermal stability studies: TGA studies indicated that both $Zn_3V_2TeO_{10}$ and $Cd_4V_2Te_3O_{15}$ are thermally stable up to

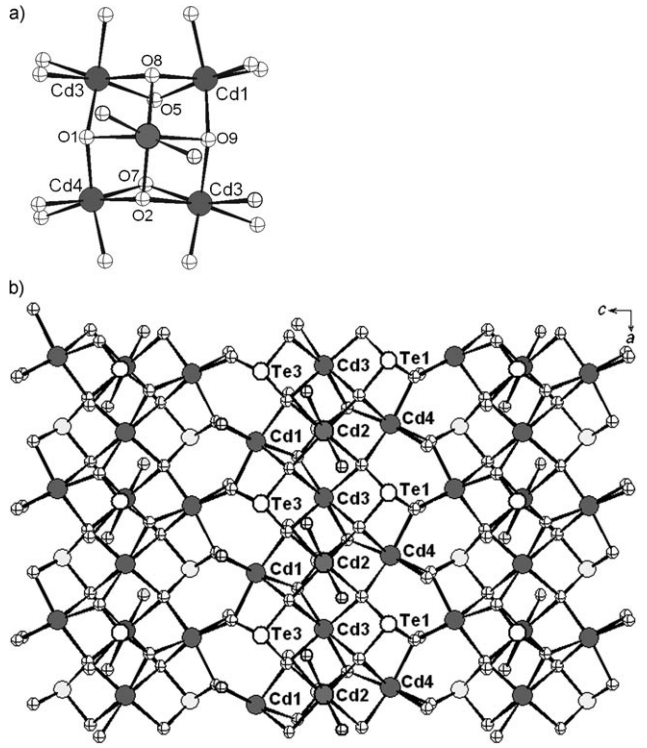

Figure 5. A $\{Cd_5O_{20}\}$ pentamer (a) and a cadmium(II) tellurium(IV) oxide layer in $Cd_4V_2Te_3O_{15}$ (b).

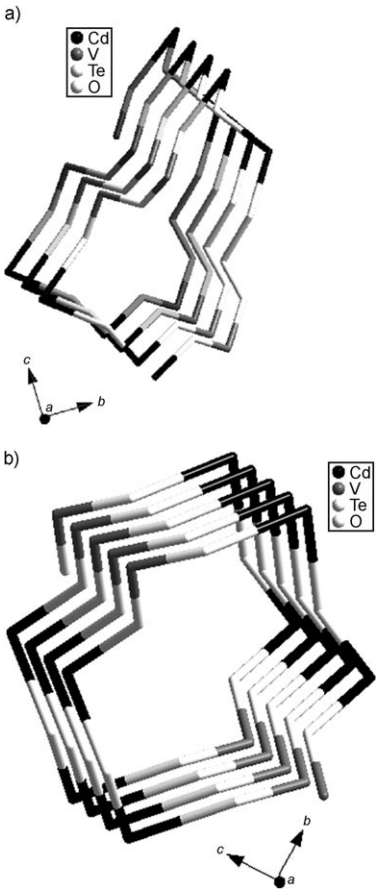

Figure 6. Left-handed helical tunnels along the *a* axis in $Cd_4V_2Te_3O_{15}$. a) based on Cd_4V_3Te eight-membered rings and b) based on Cd_4V_2 six-membered rings.

about 840 °C (Figure 7). Both compounds exhibit only one main step of weight loss. The total weight losses at 1300 °C are 27.4 % and 70.5 %, for $Zn_3V_2TeO_{10}$ and $Cd_4V_2Te_3O_{15}$, respectively. For $Zn_3V_2TeO_{10}$, the weight loss is expected to correspond to the release of one TeO_2 molecule per formula unit (calculated weight loss 27.2 %). For $Cd_4V_2Te_3O_{15}$, the weight loss is much larger than the calculated value for the release of three TeO_2 molecules per formula unit (calculated weight loss 40.8 %) and we still cannot fully understand the thermal decomposition process of this compound. The final residues were not characterized due to their melting with the TGA bucket made of Al_2O_3 under such high temperature.

Differential thermal analysis: The DTA trace for $Cd_4V_2Te_3O_{15}$ exhibits an endothermic peak at 751 °C in the heating curve and an exothermic peak at 695 °C in the cooling curve (Figure 8), indicating that $Cd_4V_2Te_3O_{15}$ melts congruently at 751 °C. To further confirm that $Cd_4V_2Te_3O_{15}$ melts congruently, a 300 mg powdered sample of $Cd_4V_2Te_3O_{15}$ was packed into a crucible, was heated to 820 °C, was held at this temperature for 30 min, and was then rapidly cooled to room temperature. The measured powder XRD pattern of the resultant solidified melt is essentially identical to that of the initial $Cd_4V_2Te_3O_{15}$ powder (see Supporting Information). Therefore, in principle, large single crystals could be grown from the stoichiometric melts.[3]

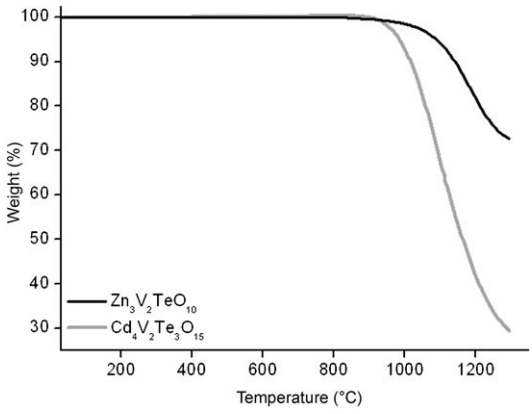

Figure 7. TGA curves for $Zn_3V_2TeO_{10}$ and $Cd_4V_2Te_3O_{15}$.

Optical properties: Optical diffuse reflectance spectrum studies indicate that $Zn_3V_2TeO_{10}$ and $Cd_4V_2Te_3O_{15}$ are semiconductors with an optical band gap of 2.96 eV and 2.66 eV, respectively (Figure 9). UV absorption spectra of $Zn_3V_2TeO_{10}$ and $Cd_4V_2Te_3O_{15}$ show little absorption in the range of 600–2500 nm (0.6–2.5 μm) and IR studies indicate that they are transparent in the range of 4000–1000 cm^{-1} (2.5–10.0 μm) (one moderate peak at 1010 cm^{-1} for

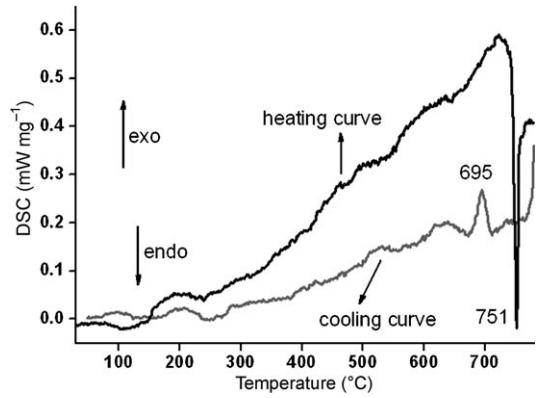

Figure 8. DTA curves of $Cd_4V_2Te_3O_{15}$ recorded at a heating rate of 5 °C min^{-1}.

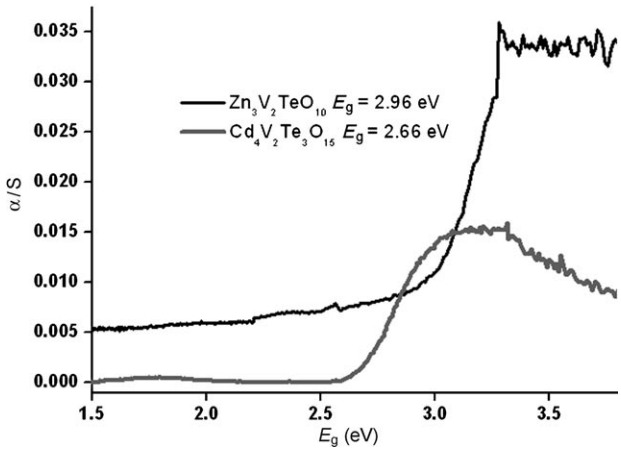

Figure 9. Optical diffuse reflectance spectra for $Zn_3V_2TeO_{10}$ and $Cd_4V_2Te_3O_{15}$.

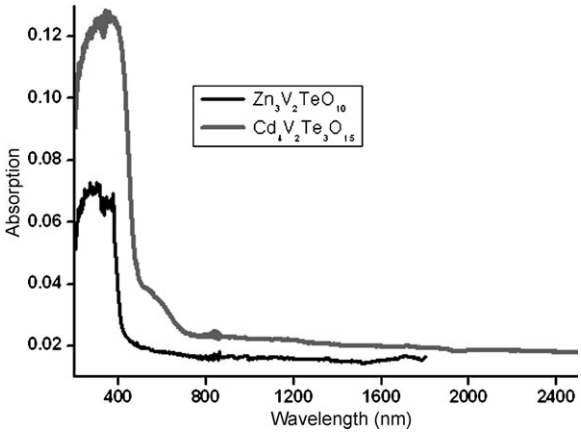

Figure 10. UV absorption spectra of $Zn_3V_2TeO_{10}$ and $Cd_4V_2Te_3O_{15}$.

$Zn_3V_2TeO_{10}$) (Figures 10 and 11). The IR absorption bands at 916, 893, 868, 850, and 815 cm^{-1} for $Cd_4V_2Te_3O_{15}$, and 1010, 976, 945, 930, 885, 839, and 808 cm^{-1} for $Zn_3V_2TeO_{10}$ are due to ν(V=O) or ν(V-O-V) vibrations, whereas those at 795, 781, 755, 742, 709, 681, 647, 629, 591, 551, 486, 450, 431, and 412 cm^{-1} for $Cd_4V_2Te_3O_{15}$, and 793, 764, 696, 553, 513,

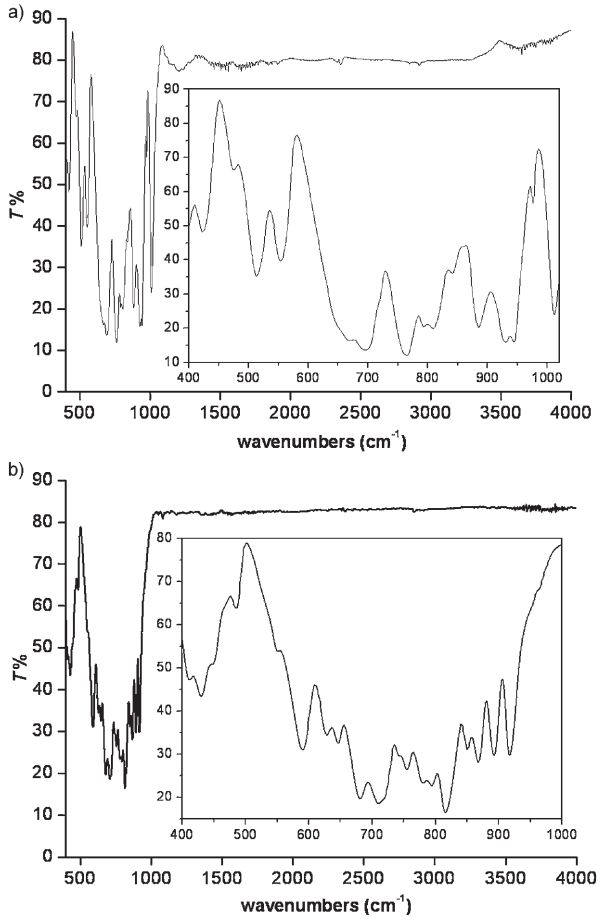

Figure 11. The infrared spectra of $Zn_3V_2TeO_{10}$ (a) and $Cd_4V_2Te_3O_{15}$ (b).

478, 422, and 411 cm^{-1} for $Zn_3V_2TeO_{10}$ can be assigned to the vibrations of ν(V–O), ν(Te–O), ν(Te-O-Te), and ν(Te-O-V).[14] Hence, both compounds are transparent in the range of 0.6–10.0 μm. The emission spectra of $Zn_3V_2TeO_{10}$ and $Cd_4V_2Te_3O_{15}$ show broad emission bands at 424 and 436 nm, respectively, under excitation at 295 nm (Figure 12),

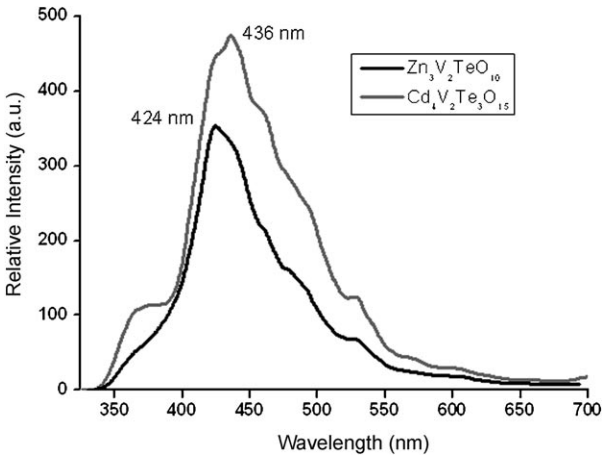

Figure 12. Emission spectra of $Zn_3V_2TeO_{10}$ and $Cd_4V_2Te_3O_{15}$ under λ_{ex} = 295 nm.

which may be attributed to the ligand-to-metal charge transfer (LMCT).[15]

Second harmonic generation (SHG) measurements: $Cd_4V_2Te_3O_{15}$ is acentric with a space group of $P2_12_12_1$. Hence, its second-order NLO properties are worth studying. SHG measurements on a Q-switched Nd:YAG laser on the sieved-powder sample (80–100 mesh) reveal that $Cd_4V_2Te_3O_{15}$ displays a moderate–strong SHG signal about 1.4 times that of KDP. This SHG response could be attributed to both the lone pairs of the tellurite anions and the 1D vanadium(V) oxide helical chain.[7,16]

Theoretical studies: The calculated band structures of $Zn_3V_2TeO_{10}$ and $Cd_4V_2Te_3O_{15}$ along high-symmetry points of the first Brillouin zone are plotted in Figure 13. It is found that the tops of the valence bands (VBs) are almost flat, whereas the bottom of the conduction bands (CBs) display small dispersion for both compounds. The state energies (eV) of the lowest conduction band (L-CB) and the highest valence band (H-VB) at some k points of both the compounds are listed in Table 3. Both the tops of the valence bands (VB) and the bottom of the conduction bands are located at the G point with a band gap of 2.95 eV and 1.94 eV, respectively, for $Zn_3V_2TeO_{10}$ and $Cd_4V_2Te_3O_{15}$. Therefore, both $Zn_3V_2TeO_{10}$ and $Cd_4V_2Te_3O_{15}$ are direct band-gap semiconductors. The calculated band gap of $Zn_3V_2TeO_{10}$ is comparable with the experimental one (2.96 eV), whereas that of $Cd_4V_2Te_3O_{15}$ is slightly smaller than the experimental one. The discrepancy is due to the limitation of the DFT method that sometimes underestimates the band gap in semiconductors and insulators.[17] As a result, a scissors operator of 0.7 eV was applied for the calculated optical properties of $Cd_4V_2Te_3O_{15}$ to shift all the conduction levels in accordance with the measured value of the band gap.

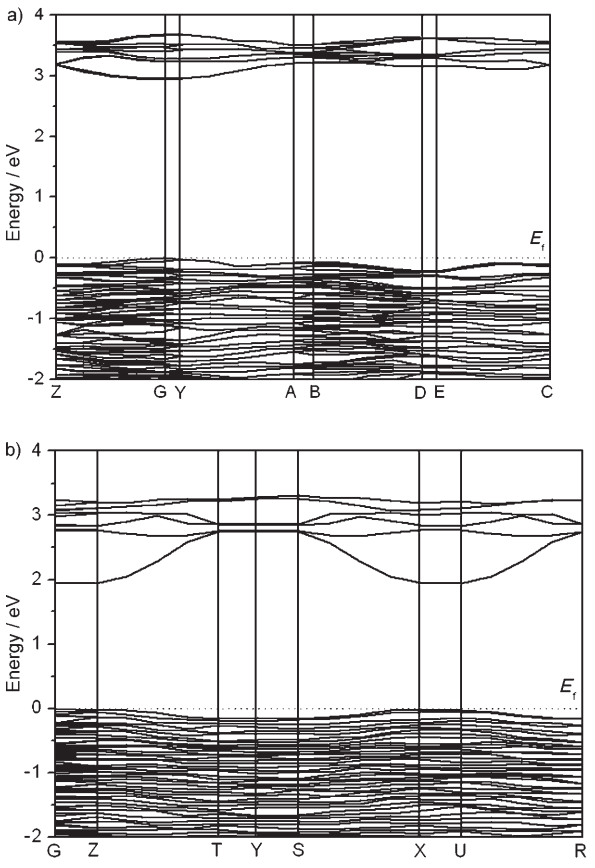

Figure 13. Band structures for the crystals $Zn_3V_2TeO_{10}$ (a) and $Cd_4V_2Te_3O_{15}$ (b) (bands are shown only between −2 and 4 eV for clarity, and the Fermi level is set at 0 eV).

The bands can be assigned according to the total and partial densities of states (TDOS and PDOS, respectively) as plotted in Figure 14. The TDOS and PDOS of both compounds are similar; the bands just above the Fermi level (the Fermi level is set at the top of the valence band) are derived from V-3d with small mixings of Te-5p and O-2p states in 2.5–4.3 eV and 1.5–3.9 eV for $Zn_3V_2TeO_{10}$ and $Cd_4V_2Te_3O_{15}$, respectively. The VB just below the Fermi level are mainly from O-2p states mixing with a small amount of the Te-5s and Te-5p states for both compounds. Accordingly, it can be considered that the optical absorptions are mainly due to the charge transfer from O-2p to V-3d states.

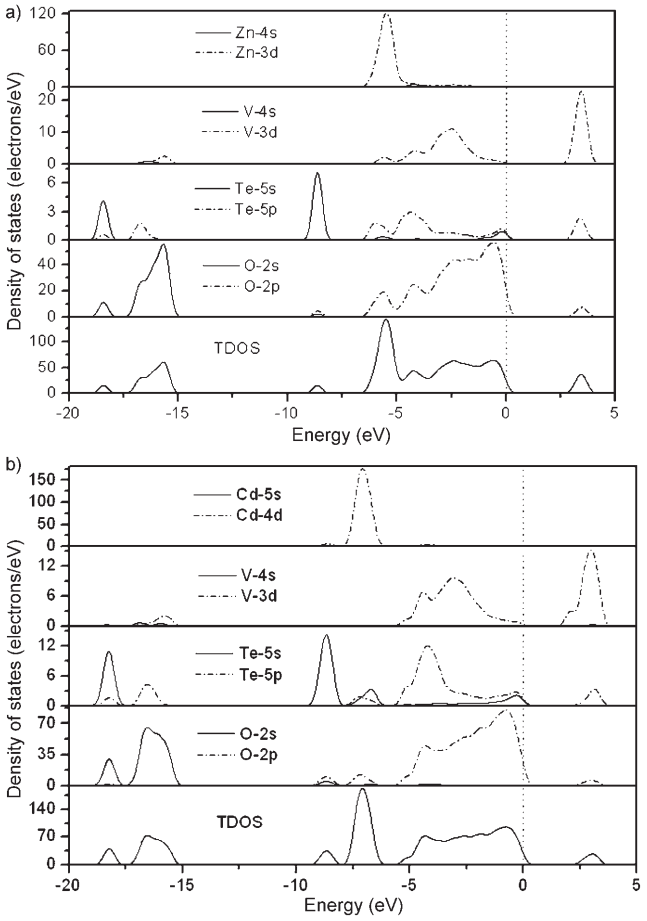

Figure 14. The total density of states and partial density of states of $Zn_3V_2TeO_{10}$ (a) and $Cd_4V_2Te_3O_{15}$ (b) (the Fermi level is set at 0 eV).

Table 2. Important bond lengths [Å] for $Zn_3V_2TeO_{10}$ and $Cd_4V_2Te_3O_{15}$.

	$Zn_3V_2TeO_{10}$		
Zn(1)−O(2)#1	1.998(4)	Zn(1)−O(3)	2.042(4)
Zn(1)−O(8)#2	2.042(5)	Zn(1)−O(7)#3	2.064(4)
Zn(1)−O(1)	2.312(5)	Zn(1)−O(4)#1	2.352(4)
Zn(2)−O(5)#4	1.905(5)	Zn(2)−O(7)#3	1.982(4)
Zn(2)−O(2)	1.987(4)	Zn(2)−O(6)#5	2.024(5)
Zn(2)−O(1)	2.462(4)	Zn(3)−O(3)	1.941(4)
Zn(3)−O(9)#6	2.009(4)	Zn(3)−O(10)#7	2.017(4)
Zn(3)−O(10)#3	2.093(4)	Zn(3)−O(9)#1	2.329(4)
V(1)−O(5)	1.661(5)	V(1)−O(6)	1.670(5)
V(1)−O(7)	1.733(5)	V(1)−O(1)	1.817(4)
V(2)−O(8)	1.641(5)	V(2)−O(9)	1.688(4)
V(2)−O(10)	1.730(4)	V(2)−O(4)	1.805(5)
Te(1)−O(2)	1.866(4)	Te(1)−O(3)	1.894(4)
Te(1)−O(4)	2.058(4)	Te(1)−O(1)	2.085(4)
	$Cd_4V_2Te_3O_{15}$		
Cd(1)−O(3)#1	2.164(7)	Cd(1)−O(5)#2	2.188(8)
Cd(1)−O(10)	2.306(7)	Cd(1)−O(9)#3	2.329(8)
Cd(1)−O(8)	2.433(8)	Cd(1)−O(13)#3	2.455(7)
Cd(2)−O(2)#4	2.169(7)	Cd(2)−O(8)#5	2.199(8)
Cd(2)−O(14)#5	2.256(8)	Cd(2)−O(15)	2.355(8)
Cd(2)−O(9)	2.415(8)	Cd(2)−O(1)#6	2.500(8)
Cd(3)−O(7)#7	2.267(8)	Cd(3)−O(5)#7	2.274(8)
Cd(3)−O(1)	2.320(7)	Cd(3)−O(9)#2	2.357(7)
Cd(3)−O(2)	2.581(8)	Cd(3)−O(8)#2	2.615(8)
Cd(4)−O(10)#1	2.161(7)	Cd(4)−O(7)#8	2.219(7)
Cd(4)−O(3)	2.259(8)	Cd(4)−O(1)#9	2.267(8)
Cd(4)−O(4)#10	2.437(8)	Cd(4)−O(2)#11	2.438(8)
V(1)−O(13)#3	1.633(7)	V(1)−O(11)#12	1.638(8)
V(1)−O(12)#13	1.804(8)	V(1)−O(12)	1.818(8)
V(2)−O(4)	1.663(8)	V(2)−O(14)	1.683(7)
V(2)−O(15)	1.692(8)	V(2)−O(6)	1.860(8)
Te(1)−O(3)#12	1.862(7)	Te(1)−O(2)	1.888(7)
Te(1)−O(1)	1.888(7)	Te(1)−O(4)#14	2.525(8)
Te(2)−O(7)	1.854(8)	Te(2)−O(5)#3	1.875(8)
Te(2)−O(6)	1.943(8)	Te(3)−O(10)	1.867(7)
Te(3)−O(8)	1.883(8)	Te(3)−O(9)	1.909(8)

Symmetry transformations used to generate equivalent atoms: For $Zn_3V_2TeO_{10}$: #1: $x+1,y,z$; #2: $x+1,y,z-1$; #3: $x,y,z-1$; #4: $-x+1,-y+1,-z+1$; #5: $x-1,y,z-1$; #6: $x+1,-y+3/2,z-1/2$; #7: $x,-y+3/2,z-1/2$. For $Cd_4V_2Te_3O_{15}$: #1: $x-1/2,-y+1/2,-z+1$; #2: $-x+1,y-1/2,-z+3/2$; #3: $x-1,y,z$; #4: $-x+1,y+1/2,-z+3/2$; #5: $x+1,y,z$; #6: $-x+2,y+1/2,-z+3/2$; #7: $x,y-1,z$; #8: $x,y-1,z-1$; #9: $x-1,y,z-1$; #10: $-x+1/2,-y+1,z-1/2$; #11: $x,y,z-1$; #12: $x,y,z+1$; #13: $x-1/2,-y+3/2,-z+2$; #14: $-x+3/2,-y+1,z+1/2$.

density of the Zn-3d (Cd-4d) state are larger than those of the O-2p state in the range from −4.7 to −6.7 eV (−5.9 to −8.0 eV for $Cd_4V_2Te_3O_{15}$), whereas the densities of V-3d and Te-5p states are much smaller than those of the O-2p state from −3.6 to −6.7 eV (Fermi energy to −5.8 eV for $Cd_4V_2Te_3O_{15}$), which indicate that the V−O and Te−O bonds are mainly covalent in nature, whereas the Zn−O or Cd−O bonds have more ionic characters.

Semi-empirical population analyses allow a more quantitative bond analysis. The calculated bond orders of Zn−O, V−O, and Te−O bonds are −0.03–0.37 e, 0.57–0.92 e, and 0.27–0.54 e, respectively, for $Zn_3V_2TeO_{10}$, whereas those for Cd−O, V−O, and Te−O bonds are 0.06–0.24 e, 0.52–0.88 e, and 0.40–0.56 e, respectively, for $Cd_4V_2Te_3O_{15}$ (covalent single-bond order is generally 1.0 e), respectively (Supporting Information). Accordingly, we can also say that the covalent character of the V−O bond is greater than that of the Te−O bond, and the ionic character of the Zn−O or Cd−O bond is greater than that of the Te−O bond.

Particularly, for $Zn_3V_2TeO_{10}$, the VB from −6.9 eV to the Fermi level mainly originates from Zn-3d, O-2p, V-3d, with a small mixing with Te-5p states, whereas the VB ranging from −7.9 to −9.3 eV is composed of the states of Te-5s and O-2s states. The states of O-2s mixing with small amounts of Te-5s, Te-5p, and V-3d states form the VB lying from −14.8 to −19.1 eV. For $Cd_4V_2Te_3O_{15}$, the VB from −5.8 eV to the Fermi level mainly originates from O-2p, Te-5p, and V-3d states, whereas the states of Cd-4d, Te-5s, O-2p mixing with small amounts of Te-5p and O-2s states dominate the VB ranging from −5.9 to −9.5 eV. The band from −19.0 to −15.0 eV originates mainly from Te-5s states and O-2s states, as well as a small portion of Cd-5s, V-3d, Te-5p, and O-2p states.

The atomic site and angular momentum projected densities of states (DOS) of the two compounds allow us to elucidate the nature of the electronic band structures and chemical bonds. As shown in Figure 12, it can be noted that the

More insights into the electronic structures can be obtained by performing more detailed optical-property calculations. The optical functions reflect the fine structure of the energy distribution of the electron states in the valence and conduction bands. Figure 15 shows the imaginary parts of the dielectric functions of $Zn_3V_2TeO_{10}$ and $Cd_4V_2Te_3O_{15}$. The dielectric functions are composed of three parts: $\varepsilon_{2x}(\omega)$, $\varepsilon_{2y}(\omega)$, and $\varepsilon_{2z}(\omega)$, which correspond to those in the x, y, and z directions, respectively. The anisotropy is especially evident in the highest of the peaks. The average function, $\varepsilon_2(\omega)=(\varepsilon_{2x}+\varepsilon_{2y}+\varepsilon_{2z})/3$, is shown in Figure 16. The highest peaks are located at 3.90 and 6.4 eV, respectively, for $Zn_3V_2TeO_{10}$ and $Cd_4V_2Te_3O_{15}$, both originating mainly from the O-2p to V-3d direct interband transitions. The average values of polarized zero-frequency dielectric constants is $\varepsilon(0)=(\varepsilon_x+\varepsilon_y+\varepsilon_z)/3=2.08$ and 3.91, respectively, for $Zn_3V_2TeO_{10}$ and $Cd_4V_2Te_3O_{15}$. The dispersion of linear refractive index is shown in Figure 17. The anisotropy of the refractive index resulted from the aniso-

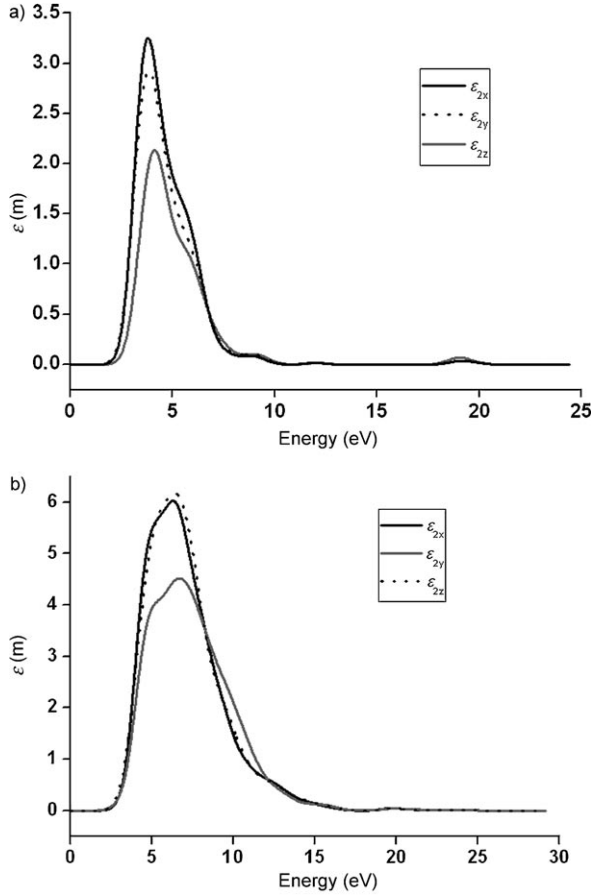

Figure 15. The calculated imaginary parts of the dielectric functions of $Zn_3V_2TeO_{10}$ (a) and $Cd_4V_2Te_3O_{15}$ (b) in the polarization along the *x*, *y*, and *z* directions.

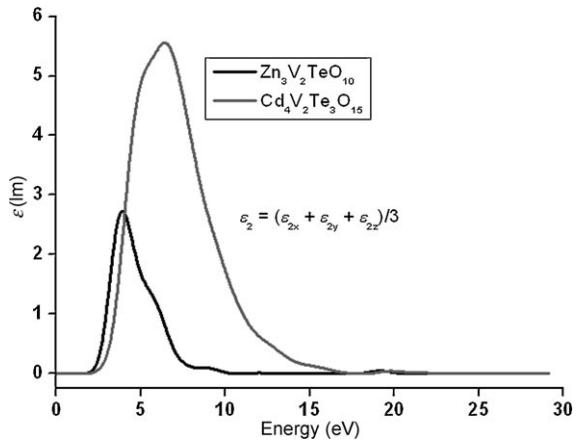

Figure 16. Average values over the three Cartesian directions of calculated imaginary parts of the dielectric functions for $Zn_3V_2TeO_{10}$ and $Cd_4V_2Te_3O_{15}$.

tropy of the dielectric function, $n^z > n^y > n^x$ and $n^z > n^x > n^y$ for $Zn_3V_2TeO_{10}$ and $Cd_4V_2Te_3O_{15}$, respectively.

The refractive index is linked with the dielectric constants by the relation of $n^2(\omega) = \varepsilon(\omega)$. The calculated dielectric constants of static case $\varepsilon(0)$ and the refractive indexes *n* at

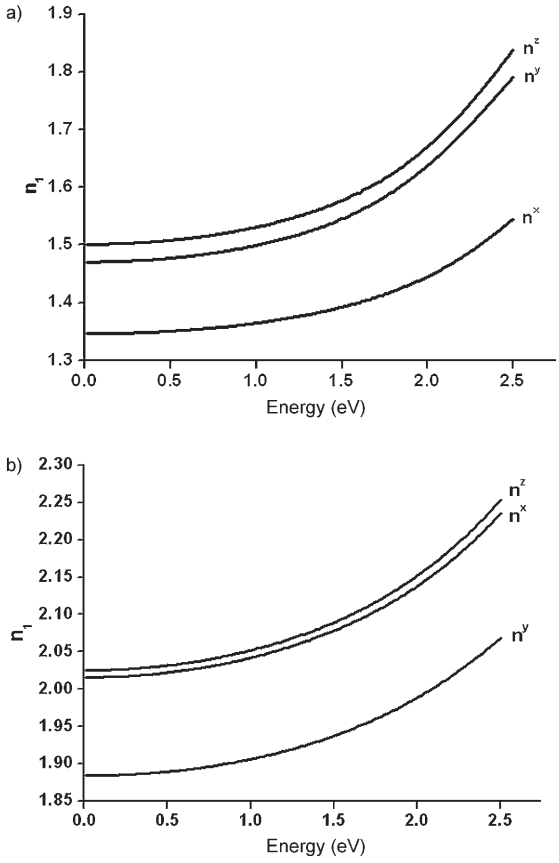

Figure 17. Calculated linear refractive indices for $Zn_3V_2TeO_{10}$ (a) and $Cd_4V_2Te_3O_{15}$ (b).

1064 nm in the *x*, *y*, and *z* directions are listed in Table 4. Because the refractive indexes of $Zn_3V_2TeO_{10}$ and $Cd_4V_2Te_3O_{15}$ have not been reported and there are no experimental data concerning the refractive indices of metal tellurite crystals, our calculated results can only be compared with the observed results of the other tellurite glasses. It is reported that the observed refractive index of tellurite

Table 3. The state energies [eV] of the lowest conduction band (L-CB) and the highest valence band (H-VB) at some *k* points of the crystal $Zn_3V_2TeO_{10}$ and $Cd_4V_2Te_3O_{15}$.

Compound	*k* point	L-CB	H-VB
$Zn_3V_2TeO_{10}$	Z (0.000, 0.000, 0.500)	3.17535	−0.10989
	G (0.000, 0.000, 0.000)	2.94854	0
	Y (0.000, 0.500, 0.000)	2.95077	−0.02041
	A (−0.500, 0.500, 0.000)	3.21338	−0.07864
	B (−0.500, 0.000, 0.000)	3.20226	−0.07024
	D (−0.500, 0.000, 0.500)	3.14717	−0.21784
	E (−0.500, 0.5000, 0.500)	3.14750	−0.21753
	C (0.000, 0.500, 0.500)	3.18275	−0.11068
$Cd_4V_2Te_3O_{15}$	G (0.000, 0.000, 0.000)	1.93718	0
	Z (0.000, 0.000, 0.500)	1.94553	−0.02672
	T (−0.500, 0.000, 0.500)	2.74844	−0.16030
	Y (−0.500, 0.000, 0.000)	2.74771	−0.15014
	S (−0.500, 0.500, 0.000)	2.74603	−0.15942
	X (0.000, 0.500, 0.000)	1.94814	−0.01390
	U (0.000, 0.500, 0.500)	1.94567	−0.02751
	R (−0.500, 0.500, 0.500)	2.75005	−0.16855

glasses are generally 2.1 at 400–700 nm.[18] Therefore, our calculated refractive indexes in the range of 400–700 nm of both compounds may be slightly underestimated or comparative.

Conclusion

Our exploration of the new type of second-order NLO materials of Zn(Cd)-V^{V}-Te^{IV}-O systems resulted in two new quaternary compounds, namely, $Zn_3V_2TeO_{10}$ and $Cd_4V_2Te_3O_{15}$. Both compounds are highly thermally stable and they are semiconductors. Moreover, $Cd_4V_2Te_3O_{15}$ displays a moderately strong SHG signal of about 1.4 times that of KDP. It is transparent in the IR region and theory indicates that large crystals could be grown from the stoichiometric melts. It is believed that the SHG efficiency of this compound could be improved if VO_4 tetrahedra are replaced by MoO_6 or VO_6 octahedra which display much larger second-order Jahn–Teller distortions. We also believe that other new second-order NLO materials transparent in the IR region can be found in other related systems that combine d^0 cations susceptible to second-order Jahn–Teller distortion and cations with stereoactive lone pairs, such as, Zn(Cd)-Mo^{VI}(W^{VI})-Te^{IV}(Se^{IV})-O systems and we are currently exploring these possibilities.

Experimental Section

Materials and methods: All of the chemicals were analytically pure, obtained from commercial sources, and used without further purification. Transition-metal oxides were purchased from the Shanghai Reagent Factory and TeO_2 (99+%) was purchased from ACROS ORGANICS. IR spectra were recorded by using a Magna 750 FTIR spectrometer with samples as KBr pellets in the range of 4000–400 cm^{-1}. Microprobe elemental analyses were performed by using a field-emission scanning electron microscope (FESEM, JSM6700F) equipped with an energy-dispersive X-ray spectroscope (EDS, Oxford INCA). X-Ray powder diffraction (XRD) patterns were collected on an XPERT-MPD θ-2θ diffractometer by using graphite-monochromated $Cu_{K\alpha}$ radiation in the angular range $2\theta = 5$–$85°$ with a step size of 0.05°. Optical diffuse reflectance spectra were measured at room temperature with a Perkin–Elmer Lambda 900 UV/Vis spectrophotometer. A $BaSO_4$ plate was used as a standard (100% reflectance). The absorption spectrum was calculated from reflectance spectra by using the Kubelka–Munk function: $\alpha/S = (1-R)^2/2R$,[19] where α is the absorption coefficient, S is the scattering coefficient which is practically independent of wavelength when the particle size is larger than 5 μm, and R is the reflectance. Thermogravimetric analyses were conducted by using a NETZSCH STA 449C unit at a heating rate of 5 °C min^{-1} under a static air atmosphere. Differential thermal analysis (DTA) was performed under N_2 by using a NETZSCH DTA404PC instrument. The sample and reference (Al_2O_3) were placed in Pt crucibles, heated from room temperature to 780 °C, and then cooled to room temperature at a rate of 5 °C min^{-1}. Photoluminescence analyses were performed on a Perkin–Elemer LS55 fluorescence spectrometer. The measurement of the powder frequency-doubling effect was carried out on the sieved (80–100 mesh) powder sample of $Cd_4V_2Te_3O_{15}$ by means of the modified method of Kurtz and Perry.[20] The fundamental wavelength was 1064 nm that was generated by a Q-switched Nd:YAG laser. The SHG wavelength was 532 nm. Sieved KDP powder (80–100 mesh) was used as a reference.

Computational descriptions: Single-crystal structural data of the two compounds were used for the theoretical calculations. Band structures, DOS, and optical property calculations were performed with the total-energy code CASTEP.[21] The total energy was calculated by using density functional theory (DFT) by employing the Perdew–Burke–Ernzerhof generalized gradient approximation.[22] The interactions between the ionic cores and the electrons were described by the norm-conserving pseudopotential.[23] The following orbital electrons were treated as valence electrons: Zn-$3d^{10}4s^2$, Cd-$4d^{10}5s^2$, V-$3d^34s^2$, Te-$5s^25p^4$, and O-$2s^22p^4$. Considering the balance of computational cost and precision, we chose a cutoff energy of 460 eV and a 4×1×4 Monkhorst–Pack k-point sampling for $Zn_3V_2TeO_{10}$, a cutoff energy of 450 eV and a 4×1×1 (5×2×2 for optical properties) Monkhorst–Pack k-point sampling for $Cd_4V_2Te_3O_{15}$. The calculations of optical properties for $Cd_4V_2Te_3O_{15}$ used 96 empty bands. The other calculation parameters and convergent criteria were the default values of the CASTEP code.

The calculations of linear optical properties in terms of the complex dielectric function $\varepsilon(\omega) = \varepsilon_1(\omega) + i\varepsilon_2(\omega)$ were made. $\varepsilon_2(\omega)$ can be thought of as detailing the real transitions between occupied and unoccupied electronic states. The imaginary part of the dielectric function ε_2 was given by Equation (3):[24]

$$\varepsilon_2^{ij}(\omega) = 8\pi^2\hbar^2e^2/(m^2V)\sum_k\sum_{cv}(f_c - f_v)p_{cv}^i(k)p_{cv}^j(k)/(E_{cv}{}^2)\sigma[E_c(k) - E_v(k) - \hbar\omega] \quad (3)$$

where $\delta[E_c(k) - E_v(k) - \hbar\omega]$ denotes the energy difference between the conduction and valence bands at the k point with the absorption of a quantum $\hbar\omega$. The f_c and f_v represent the Fermi distribution functions of the conduction and valence bands, respectively. The term $p_{cv}^i(k)$ denotes the momentum matrix element transition from the energy level c of the conduction band to the level v of the valence band at the k point in the Brillouin zones, and V is the volume of the unit cell. The m, e, and $\hbar$ are the electron mass, charge, and the Planck constant, respectively.

The real part $\varepsilon_1(\omega)$ of the dielectric function $\varepsilon(\omega)$ follows from the Kramer–Kronig relationship. All the other optical constants may be derived from $\varepsilon_1(\omega)$ and $\varepsilon_2(\omega)$.[25] For example, the refractive index $n(\omega)$ can be calculated by using expression (4) :

$$n(\omega) = \left(\frac{1}{\sqrt{2}}\right)\left[\sqrt{\varepsilon_1^2(\omega) + \varepsilon_2^2(\omega) + \varepsilon_1(\omega)}\right]^{1/2} \quad (4)$$

Preparation of $Zn_3V_2TeO_{10}$: Brick-red plate-shaped single crystals of $Zn_3V_2TeO_{10}$ were initially prepared by the solid-state reaction of a mixture containing ZnO (0.130 g, 1.6 mmol), V_2O_5 (0.146 g, 0.8 mmol), and TeO_2 (0.128 g, 0.8 mmol) in an evacuated quartz tube at 700 °C, for six days, and was then cooled to 300 °C at 5 °C h^{-1} before switching off the furnace. The atomic ratio of Zn/V/Te determined by energy-dispersive spectrometry (EDS) was 2.7:2.1:1.0, which was in good agreement with that determined from structural analysis by using single-crystal X-ray diffraction. After proper structural analysis, a pure powder sample of $Zn_3V_2TeO_{10}$ was obtained quantitatively by the solid-state reaction of a mixture of $ZnO/V_2O_5/TeO_2$ in a molar ratio of 3:1:1 at 670 °C for six days. Its purity was confirmed by XRD powder diffraction studies (see Supporting Information). IR (KBr): $\tilde{\nu}$ = 1010 (m), 976 (w), 945 (s), 930 (s), 885 (s), 839 (m), 808 (s), 793 (s), 764 (s), 696 (s), 553 (m), 513 (m), 478 (w), 422 (w), 411 cm^{-1} (w).

Preparation of $Cd_4V_2Te_3O_{15}$: Single crystals of $Cd_4V_2Te_3O_{15}$ (needle in shape and light-yellow in color) were obtained containing CdO (0.141 g, 1.1 mmol), V_2O_5 (0.100 g, 0.55 mmol), and TeO_2 (0.088 mg, 0.55 mmol) by using a similar method. The reaction mixture was thoroughly ground and pressed into a pellet, which was then put into a quartz tube which was evacuated and sealed. The quartz tube was heated at 720 °C for six days and was then cooled to 320 °C at 4 °C h^{-1} before switching off the furnace. The measured molar ratio of Cd/V/Te of 3.8:2.1:3.0 by using energy-dispersive spectrometry (EDS) microprobe analysis was in good agreement with that determined by using X-ray single-crystal diffraction measurements. A pure powder sample of $Cd_4V_2Te_3O_{15}$ could be prepared

quantitatively by the solid-state reaction of a mixture of $CdO/V_2O_5/TeO_2$ in a molar ratio of 4:1:3 at 610 °C for six days. Its purity was confirmed by XRD powder diffraction studies (see Supporting Information). IR (KBr): $\tilde{\nu}$ = 916 (s), 893 (s), 868 (s), 850 (s), 815 (s), 795 (s), 781 (s), 755 (s), 742 (s), 709 (s), 681 (s), 647 (s), 629 (s), 591 (s), 551 (m), 486 (w), 450 (m), 431 (m), 412 cm^{-1} (m).

X-ray crystallography: Data was collected for both compounds by using a Rigaku Mercury CCD diffractometer equipped with graphite-monochromated $Mo_{K\alpha}$ radiation (λ = 0.71073 Å), at 293 K. The data sets were corrected for Lorentz and polarization factors, as well as for absorption by the Multi-scan method.[26a] Both structures were solved by the direct method and refined by full-matrix least-squares fitting on F^2 by SHELX-97.[26b] All atoms were refined with anisotropic thermal parameters. Crystallographic data and structural refinements for both the compounds are summarized in Table 1. Important bond lengths are listed in Table 2.

Table 4. Calculated dielectric constants of static case and refractive indices at 1064 nm in different polarization directions.

Compound	Scissor operator [eV]	$\varepsilon_x(0)$	$\varepsilon_y(0)$	$\varepsilon_z(0)$	n_x	n_y	n_z
$Zn_3V_2TeO_{10}$	0	2.2537	2.1626	1.8126	1.54	1.51	1.37
$Cd_4V_2Te_3O_{15}$	0.7	4.0646	3.5508	4.1024	2.05	1.91	2.06

Further details of the crystal structure investigations may be obtained from the Fachinformationszentrum Karlsruhe, 76344 Eggenstein-Leopoldshafen, Germany (Fax: (+49) 7247-808-666; e-mail: crysdata@fiz-karlsruhe.de) on quoting the depository numbers CSD-418558 and CSD-418184.

Acknowledgements

This work was supported by the National Natural Science Foundation of China (Nos. 20731006, 20573113, and 20521101) and the Knowledge Innovation Program of the Chinese Academy of Sciences. We thank Prof. Ding Li for his great help with the SHG measurements.

[1] C. Chen, G. Liu, *Annu. Rev. Mater. Sci.* **1986**, *16*, 203–243.
[2] a) P. Becker, *Adv. Mater.* **1998**, *10*, 979–992; b) C.-T. Chen, Y.-B. Wang, B.-C. Wu, K.-C. Wu, W.-L. Zeng, L.-H. Yu, *Nature* **1995**, *373*, 322–324; c) C.-T. Chen, B.-C. Wu, A. D. Jiang, G. M. You, *Sci. Sin. Ser. B (Engl. Ed.)* **1985**, *18*, 235–243; d) M. E. Hagerman, K. R. Poeppelmeier, *Chem. Mater.* **1995**, *7*, 602–621; e) P. S. Halasyamani, K. R. Poeppelmeier, *Chem. Mater.* **1998**, *10*, 2753–2769.
[3] S. L. Pan, J. P. Smit, B. Watkins, M. R. Marvel, C. L. Stern, K. R. Poeppelmeier, *J. Am. Chem. Soc.* **2006**, *128*, 11631–11634.
[4] a) H.-S. Ra, K.-M. Ok, P. S. Halasyamani, *J. Am. Chem. Soc.* **2003**, *125*, 7764–7765; b) K.-M. Ok, P. S. Halasyamani, *Inorg. Chem.* **2004**, *43*, 4248–4253; c) Y. Porter, K.-M. Ok, N. S. P. Bhuvanesh, P. S. Halasyamani, *Chem. Mater.* **2001**, *13*, 1910–1915; d) Y. Porter, N. S. P. Bhuvanesh, P. S. Halasyamani, *Inorg. Chem.* **2001**, *40*, 1172–1175.
[5] a) R. T. Hart, K.-M. Ok, P. S. Halasyamani, J. W. Zwanziger, *Appl. Phys. Lett.* **2004**, *85*, 938–939; b) J. Goodey, J. Broussard, P. S. Halasyamani, *Chem. Mater.* **2002**, *14*, 3174–3180.
[6] a) M. G. Johnston, W. T. A. Harrison, *Inorg. Chem.* **2001**, *40*, 6518–6520; b) V. Balraj, K. Vidyasagar, *Inorg. Chem.* **1999**, *38*, 5809–5813; c) W. T. A. Harrison, L. L. Dussack, A. J. Jacobson, *Inorg. Chem.* **1994**, *33*, 6043–6049; d) P. M. Almond, T. E. Albrecht-Schemitt, *Inorg. Chem.* **2002**, *41*, 1177–1183.
[7] a) K.-M. Ok, P. S. Halasyamani, *Chem. Mater.* **2006**, *18*, 3176–3183; b) E. O. Chi, K.-M. Ok, Y. Porter, P. S. Halasyamani, *Chem. Mater.* **2006**, *18*, 2070–2074; c) F. Kong, S.-P. Huang, Z.-M. Sun, J.-G. Mao, W.-D. Cheng, *J. Am. Chem. Soc.* **2006**, *128*, 7750–7751.
[8] a) Y.-U. Kwon, K.-S. Lee, Y. H. Kim, *Inorg. Chem.* **1996**, *35*, 1161–1167; b) J. T. Vaughey, W. T. A. Harrison, L. L. Dussack, A. J. Jacobson, *Inorg. Chem.* **1994**, *33*, 4370–4375; c) T. Sivakumar, K. M. Ok, P. S. Halasyamani, *Inorg. Chem.* **2006**, *45*, 3602–3605; d) K.-S. Lee, Y.-U. Kwon, H. Namgung, S.-H. Kim, *Inorg. Chem.* **1995**, *34*, 4178–4181.
[9] a) V. G. Dmitriev, G. G. Gurzadyan, D. N. Nikogosyan, *Handbook of Nonlinear Optical Crystals*, Springer, Berlin, **1991**; b) J.-H. Liao, G.-M. Marking, K. F. Hsu, Y. Matsushita, M. D. Ewbank, R. Borwick, P. Cunningham, M. J. Rosker, M. G. Kanatzidis, *J. Am. Chem. Soc.* **2003**, *125*, 9484–9493.
[10] H. L. Jiang, M. L. Feng, J. G. Mao, *J. Solid State Chem.* **2006**, *179*, 1911–1917.
[11] a) Y.-T. Kim, Y. H. Kim, K. Park, Y.-U. Kwon, V. G. Young, Jr., *J. Solid State Chem.* **2001**, *161*, 23–30; b) J.-Y. Xie, J.-G. Mao, *Inorg. Chem. Commun.* **2005**, *8*, 375–378.
[12] a) I. D. Brown, D. Altermatt, *Acta Crystallogr. Sect. B*, **1985**, *41*, 244–247; b) N. E. Brese, M. O'Keeffe, *Acta Crystallogr. Sect. B*, **1991**, *47*, 192–197.
[13] J. Galy, G. Meunier, S. Andersson, A. Åström, *J. Solid State Chem.* **1975**, *13*, 142–159.
[14] a) T. Sivakumar, K. M. Ok, P. S. Halasyamani, *Inorg. Chem.* **2006**, *45*, 3602–3605; b) K. M. Ok, J. Orzechowski, P. S. Halasyamani, *Inorg. Chem.* **2004**, *43*, 964–968; c) Y. Lu, E. B. Wang, M. Yuan, G. Y. Luan, Y. G. Li, H. Zhang, C. W. Hu, Y. G. Yao, Y. Y. Qin, Y. B. Chen, *J. Chem. Soc. Dalton Trans.* **2002**, 3029–3031; d) D. R. Xiao, S. T. Wang, E. B. Wang, Y. Hou, Y. G. Li, C. W. Hu, L. Xu, *J. Solid State Chem.* **2003**, *176*, 159–164.
[15] a) C. S. Liu, X. S. Shi, J. R. Li, J. J. Wang, X. H. Bu, *Cryst. Growth Des.* **2006**, *6*, 656–663; b) Z. G. Guo, R. Cao, X. J. Li, D. Q. Yuan, W. H. Bi, X. D. Zhu, Y. F. Li, *Eur. J. Inorg. Chem.* **2007**, 742–748.
[16] P. A. Maggard, C. L. Stern, K. R. Poeppelmeier, *J. Am. Chem. Soc.* **2001**, *123*, 7742–7743.
[17] a) R. W. Godby, M. Schluther, L. J. Sham, *Phys. Rev. B* **1987**, 36, 6497–6500; b) C. M. I. Okoye, *J. Phys. Condens. Matter* **2003**, *15*, 5945–5958; c) H. L. Jiang, F. Kong, J. G. Mao, *J. Solid State Chem.* **2007**, *180*, 1764–1769.
[18] a) S. Inoue, A. Nukui, K. Yamamoto, T. Yano, S. Shibata, M. Yamane, *J. Non-Cryst. Solids* **2003**, *324*, 133–141; b) E. Yousef, M. Hotzel, C. Rüssel, *J. Non-Cryst. Solids* **2004**, *342*, 82–88.
[19] W. M. Wendlandt, H. G. Hecht, *Reflectance Spectroscopy*, Interscience, New York, **1966**.
[20] S. W. Kurtz, T. T. Perry, *J. Appl. Phys.* **1968**, *39*, 3798–3813.
[21] a) M. D. Segall, P. L. D. Lindan, M. J. Probert, C. J. Pickard, P. J. Hasnip, S. J. Clark, M. C. Payne, *J. Phys. Condens. Matter* **2002**, *14*, 2717–2744; b) V. Milman, B. Winkler, J. A. White, C. J. Pickard, M. C. Payne, E. V. Akhmatskaya, R. H. Nobes, *Int. J. Quantum Chem.* **2000**, *77*, 895–910.
[22] J. P. Perdew, K. Burke, M. Ernzerhof, *Phys. Rev. Lett.* **1996**, *77*, 3865–3868.
[23] J. S. Lin, A. Qteish, M. C. Payne, V. Heine, *Phys. Rev. B* **1993**, *47*, 4174–4180.
[24] F. Bassani, G. P. Parravicini, *Electronic States and Optical Transitions in Solids*, Pergamon, Oxford, **1975**, pp. 149–154.
[25] a) S. Saha, T. P. Sinha, *Phys. Rev. B* **2000**, *62*, 8828–8834; b) M. Q. Cai, Z. Yin, M. S. Zhang, *Appl. Phys. Lett.* **2003**, *83*, 2805–2807.
[26] a) CrystalClear (Version 1.3.5), Rigaku Corp., Woodlands, TX (USA), **1999**; b) G. M. Sheldrick, SHELXTL, Crystallographic Software Package, SHELXTL (Version 5.1), Bruker-AXS, Madison, WI (USA), **1998**.

Received: September 12, 2007
Published online: December 11, 2007

